Optica Applicata, Vol. XXXI, No. 2, 2001

Modelling of radial steam oxidation of AlAs layers in cylindrically symmetric mesa structures of vertical-cavity surface-emitting lasers

Włodzimierz Nakwaski *, Paweł Maćkowiak

Institute of Physics, Technical University of Łódź, ul. Wólczańska 219, 93-005 Łódź, Poland.

Marek Osiński

Center for High Technology Materials, University of New Mexico, Albuquerque, 1313 Goddard SE, NM 87106-4343, USA.

During the last several years selective steam oxidation process has evolved into a key technology in fabrication of high-performance vertical-cavity surface-emitting lasers (VCSELs). In the present paper, kinetics of AlAs steam oxidation process in cylindrically symmetric VCSEL mesa structures is investigated theoretically. Compact analytical formulae describing the oxidation process are derived and discussed. The process parameters are extracted from existing experimental data. The parameters are found to be strongly dependent on the AlAs layer thickness and temperature. It is shown that significant differences exist between the predictions of the cylindrical model and those of widely used one-dimensional Cartesian model. Our detailed model can therefore be very important for achieving a good control of the oxidation process in fabrication of modern VCSELs.

1. Introduction

Selective steam oxidation process is used to transform AlAs (or AlGaAs with high AlAs content) layers into native-oxide Al_xO_y layers [1], [2] of a much lower index of refraction and much higher both a thermal conductivity and an electrical resistivity. Application of this technique to arsenide vertical-cavity surface -emitting lasers (VCSELs) has resulted in dramatic improvements of their performance [3]–[5]. During the last several years the AlAs oxidation process has evolved into a key technology in fabrication of high-performance VCSELs, mainly used for current confinement and/or in distributed Bragg reflectors. For example, in typical oxide-confined VCSELs, the oxidation is used to create a small unoxidized aperture at the very centre of much larger oxidized mesa [6]–[9].

Detailed modelling of the oxidation process can be very helpful in achieving good controllability and high yield, necessary for commercialization of oxide

* Also with the Center for High Technology Materials, University of New Mexico, Albuquerque, NM 87131, USA.

-confined VCSELs. Yet, simulation of steam oxidation in cylindrically symmetric VCSEL structures has received very little attention so far. To the best of our knowledge, there have been only two attempts to model AlAs oxidation kinetics in cylindrically symmetric mesa structures: an analytical model of KOLEY *et al.* [10] (however, full of mistakes) and a semi-analytical model of ALONZO *et al.* [11]. Therefore, the main goal of this paper is to present our simple analytical model of the process enabling introducing its dependence on temperature and layer thicknesses. The paper is organized as follows. The model is explained in Section 2. Its parameters are discussed in Section 3. Section 4 presents our results and discussion, which is followed by conclusions in Section 5.

2. The model

Our approach is based on a simple theory of one-dimensional (1D) Cartesian oxidation of silicon proposed by DEAL and GROVE [12]. The oxidation is assumed to be governed mainly by the diffusion of O (or H_2O) through already oxidized AlAs layer to the oxidation front as well as by chemical reactions that form the oxide. The whole process is therefore composed of three phases, illustrated in Fig. 1:

– transport of the oxidant from the external ambient across the interface with the oxidized layer

$$F_1 = h(C^* - C_0), \tag{1}$$

– radial diffusion of the oxidant through the oxidized region towards the oxidation front

$$F_2(r) = -D\frac{\mathrm{d}C(r)}{\mathrm{d}r}, \tag{2}$$

– chemical reactions during hydrolyzation and/or oxidation leading to formation of alumina

$$F_3 = kC_i. \tag{3}$$

In the above relations, F_1, F_2 and F_3 represent the corresponding oxidant flux densities (per unit area and unit time), h is the gas-phase transport coefficient, C^* is the equilibrium concentration of the oxidant, C_0 is the oxidant concentration at $r = R_0$, r is the radial distance from the symmetry axis, R_0 is the outer radius of the mesa, D is the diffusion constant, $C(r)$ is the distribution of oxidant concentration in the bulk of the oxidized region, k is the oxidation reaction rate, $C_i \equiv C(R_i)$, and R_i is the inner radius of the oxidized region. Under the steady-state process conditions, total fluxes of the oxidant can be assumed to be identical in all three phases

$$(\int F_1 \mathrm{d}S)_{R_0} = (\int F_2 \mathrm{d}S)_{R_i} = (\int F_3 \mathrm{d}S)_{R_i} \tag{4}$$

where $\mathrm{d}S$ is the elementary surface.

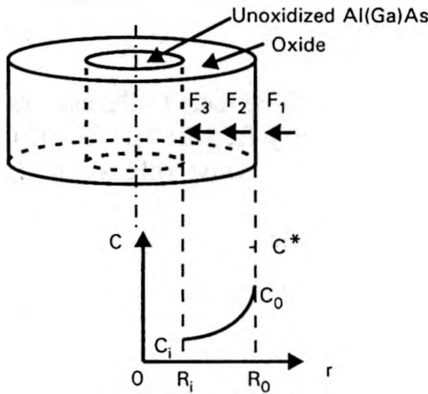

Fig. 1. Schematic illustration of the oxidation process of a cylindrical Al(Ga)As mesa.

In the Cartesian analysis, the usual assumption is that the flux $F_2(x)$ should be independent of the distance x from the interface with the ambient. For cylindrical structures, however, a more proper formulation is to require that the divergence of the flux $F_2(r)$ vanishes. This leads to the following condition for $F_2(r)$ in a layer of thickness d

$$F_2(r) = \frac{G}{2\pi r d} \tag{5}$$

where G is the total number of particles crossing any surface with $r = \text{const}$. Equation (5) immediately implies that $C(r)$ should be of the form $a + b\ln r$, with constant a and b. Besides, time evolution of the oxidized region length ρ (measured from the outer perimeter) can be written as follows [12]:

$$-\frac{\mathrm{d}\rho}{\mathrm{d}t} = \frac{F_2(r)}{N_0} \tag{6}$$

where $r = R_0 - \rho$, and N_0 is the density oxidant particles incorporated into the oxidized material.

The solution of the above system of equations, describing the oxidation kinetics in a cylindrically symmetric mesa structure, has a simple analytical form

$$Bt = (R_0 - \rho)^2 \ln\left(1 - \frac{\rho}{R_0}\right) + \rho(A + R_0) - \frac{\rho^2}{2}\left(1 + \beta\frac{A}{R_0}\right) \tag{7}$$

where t stands for the oxidation time, while the parameters β, A and B are expressed as [10], [12]:

$$\beta = \frac{k}{k+h}, \tag{8}$$

$$A = \frac{2D}{\beta h}, \tag{9}$$

$$B = \frac{2DC^*}{N_0} \tag{10}$$

It is interesting to note that in the limit of $R_0 \to \infty$, Eq. (7) reduces to the classical Deal and Grove solution valid for the Cartesian geometry (see Eq. (7) in [12]). Hence, the parameters A and B are expected to play the same role as in the Cartesian case.

Differentiation of Equation (7) gives the oxidation rate

$$\frac{d\rho}{dt} = \frac{B}{A\left(1-\beta\frac{\rho}{R_0}\right) - 2(R_0-\rho)\ln\left(1-\frac{\rho}{R_0}\right)}. \tag{11}$$

The initial rate of oxidation (at $\rho = 0$) is equal to B/A, which is again the same as in the 1D Cartesian model. The rate at the end of the oxidation process, *i.e.*, for $\rho \to R_0$, is given by $B/[A(1-\beta]$ and can be considerably greater than the initial rate if β is close to 1. At temperatures being low enough, for which

$$R_0 > \frac{\beta A}{2} \tag{12}$$

the oxidation process slows down between those two extremes to reach the minimum rate of

$$\left(\frac{d\rho}{dt}\right)_{\min} = \frac{B}{A(1-\beta)+2(R_0-\rho_{cr})} \tag{13}$$

where ρ_{cr} is the oxidation length at which the rate slows down to its minimum

$$\rho_{cr} = R_0\left\{1-\exp\left[\left(\frac{\beta A}{2R_0}\right)-1\right]\right\}. \tag{14}$$

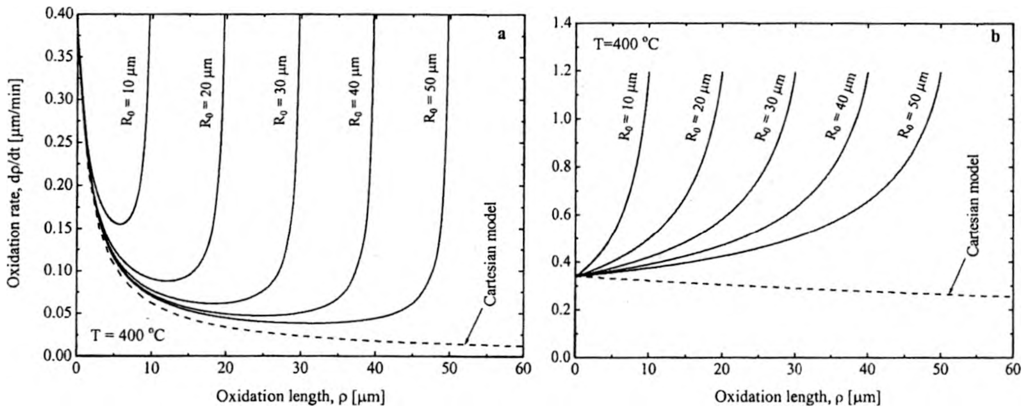

Fig. 2a,b

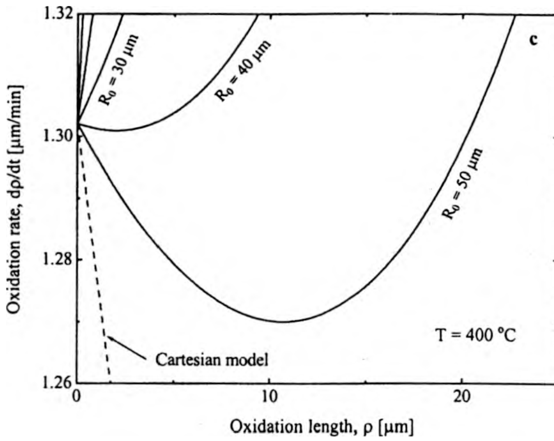

Fig. 2. Oxidation rate $d\rho/dt$ vs. oxidation length ρ for steam oxidation of AlAs at 400 °C for cylindrical mesas of various radii R_0 (solid lines), and various thicknesses of the AlAs layer: **a** – $d = 250$ nm, **b** – $d = 25$ nm, **c** – $d = 50$ nm. The values of parameters A, B and β are determined in Section 3. Each curve starts for $\rho = 0$ with the initial rate B/A and ends when $\rho = R_0$, with the final rate equal to $B/[A(1-\beta)]$. The broken line represents the 1D Cartesian solution obtained for the same values of the process parameters.

Such a behaviour is shown in Fig. 2**a** presenting plots of the oxidation rate versus oxidation length for steam oxidation of the thick ($d = 250$ nm) AlAs layer at 400 °C for cylindrical mesas of various radii R_0. In this case, $\beta A/2 = 0.562$ μm, which is less than all R_0 considered, *cf.* Eq. (12). Values of model parameters used here are determined in the next section.

Quite a different situation is at this temperature for very thin AlAs layers, for which the inequality (12) is not valid any more. Figure 2**b** shows analogous (to Fig 2**a**) curves plotted for $d = 25$ nm at 400 °C. This time $\beta A/2 = 127.4$ μm, which is higher than all R_0 considered and which immediately changes the shape of plots. The initial rate $B/A = 0.34$ μm/min becomes the minimal oxidation rate. With an increase in the oxidation length ρ the process is steadily accelerated reaching the maximum oxidation rate $B/[A(1-\beta)] = 1.19$ μm/min at the very end. Besides, a dramatically rapid rate increase at the final oxidation rate (as for $d = 250$ nm) is not observed and a significant deviation between the cylindrical and Cartesian process kinetics is clearly seen.

An intermediate case is illustrated in Fig. 2**c**, plotted for the same temperature ($T = 400$ °C), but for $d = 50$ nm this time. For this case, $\beta A/2 = 37.98$ μm, which is higher than some R_0 values considered (10 μm, 20 μm, 30 μm), but lower than remaining R_0 values (40 μm, 50 μm). The condition (12) is fulfilled for the last two R_0 values only, therefore both curves plotted for them are similar to those shown in Fig. 2**a**. All other curves are analogous to that shown in Fig. 2**b**.

The above differences result from changing the layer thickness d for the same process temperature. Nevertheless the same may be achieved by keeping the layer thickness constant and changing the temperature. For $d = 250$ nm, the critical

temperature T_{cr}, for which

$$A[d, T_{cr}(d)] = \frac{2R_0}{\beta} \tag{15}$$

is equal to 264 °C for $R_0 = 10$ μm, going down to 209 °C for $R_0 = 50$ μm. Both temperatures are lower than the process temperature (400 °C), so at this temperature the condition (12) is fulfilled for all R_0 values considered. For $d = 25$ nm, on the other hand, the critical temperature is equal to as much as 568 °C for $R_0 = 10$ μm, and is reduced to 453 °C for $R_0 = 50$ μm, which is still higher than the above process temperature. Therefore, the condition (12) is not fulfilled and all curves exhibit a monothonic increase with an increase in the oxidation length. Intermediate case is found for $d = 50$ nm. This time the critical temperatures are as follows: $T_{cr}(R_0 = 10\ \mu m) = 484$ °C, $T_{cr}(R_0 = 20\ \mu m) = 438$ °C, $T_{cr}(R_0 = 30\ \mu m) = 413$ °C, $T_{cr}(R_0 = 40\ \mu m) = 397$ °C, and $T_{cr}(R_0 = 50\ \mu m) = 385$ °C, therefore, at 400 °C, condition (12) is fulfilled only for the two largest radii, which is clearly seen in Fig. 2c.

3. The model parameters

The steam oxidation process is known to be very sensitive to temperature [13], [14]. Besides, it has been demonstrated that the oxidation process rate strongly depends on the AlAs layer thickness d [4], [5],[14] – [17]. We expect Eq. (7) to be applicable at various temperatures and for various layer thicknesses, but with appropriately adjusted values of parameters A, B, and β. In general, all three parameters can depend on temperature and layer thicknesses. However, in the absence of sufficient experimental data for cylindrical structures that could be used to determine possible variation of β with d and T, we assume β to be constant. Therefore, we use

$$\beta = 0.716 \tag{16}$$

determined only from the experimental data reported for cylindrical structures (for $d = 250$ nm and $T = 350$ °C) by KOLEY *et al.* [10]. We then use the published data for the 1D Cartesian geometry to determine $A(d, T)$ and $B(d, T)$, noting that they should coincide with the parameters used for the cylindrical geometry as long as we consider them to be independent of the mesa radius R_0.

We postulate the following form of the process parameters $\Gamma(d,T)$, where Γ stands for A or B:

$$\Gamma(d, T) = \Gamma_\infty(d)\exp\left[-\frac{E_\Gamma(d)}{k_B T}\right], \quad \Gamma = A, B, \tag{17}$$

with k_B – the Boltzmann constant. Based on the experimental data of [10], [11], [13], [14], the high-temperature limits A_∞ and B_∞ are postulated in the form

$$\Gamma_\infty(d) = \Gamma_0 \exp\left(-\frac{d}{d_{\Gamma 0}}\right), \quad \Gamma = A, B. \tag{18}$$

We find that the following form of layer thickness dependence fits well the activation energies $E_A(d)$ and $E_B(d)$

$$E_\Gamma(d) = E_{\Gamma b} + \frac{\varepsilon_{E\Gamma}}{d}, \quad \Gamma = A, B \tag{19}$$

where $E_{\Gamma b}$ represents the bulk limit of the activation energy E_Γ, $\Gamma = A, B$. The form of Eq. (19) is consistent with the layer thickness dependence of the activation energy $E_{B/A}$ for the linear rate coefficient B/A, as shown in Fig. 3 of [14]

$$E_{B/A}(d) = E_{B/A,b} + \frac{\varepsilon_{E,B/A}}{d} \tag{20}$$

with $E_{B/A,b} = 1.55$ eV and $\varepsilon_{E,B/A} = 3.96$ eV·nm. Using the data from [14] and assuming they should follow Eq. (19), we can obtain $E_{Bb} = 0.90$ eV and $\varepsilon_{EB} =$ 1.75 eV·nm. The parameters E_{Ab} and ε_{EA} are determined using

$$E_A(d) = E_B(d) - E_{B/A}(d), \tag{21}$$

which gives $E_{Ab} = -0.65$ eV and $\varepsilon_{EA} = -2.21$ eV·nm.

Table. Experimental values of parameters $A_\infty(d)$, $B_\infty(d)$ ad their best-fit counterparts satisfying Eqs. (18).

Thickness d [nm]	Parameters extracted from experimental data			Fitted parameters	
	$A_\infty(d)$ [10^{-4} μm]	$B_\infty(d)$ [10^9 μm^2/min]	References	$A_\infty(d)$ [10^{-4} μm]	$B_\infty(d)$ [10^9 μm^2/min]
25	10.45	2.3	[14]	10.52	2.213
45	7.42	1.52	[13]	7.345	1.519
100	2.36	0.37	[11]	2.731	0.540
250	0.184	0.0320	[10]	0.184	0.0322

The first three columns in the Table contain a list of parameters A_∞ and B_∞ extracted from experimental data for samples of various thicknesses. We find the remaining parameters A_0, B_0, d_{A0} and d_{B0} by fitting Eq. (18) to the data listed in columns 2 and 3 of the Table. The best fit is obtained by choosing $A_0 = 1.65\cdot10^{-3}$ μm, $B_0 = 3.54\cdot10^9$ μm^2/min, $d_{A0} = 55.6$ nm, and $d_{B0} = 53.2$ nm. The last two columns in the Table show the values of A_∞(d) and $B_\infty(d)$ calculated using Eq. (18).

4. Results and discussion

Let us examine the temperature and layer thickness dependence of the oxidation process in cylindrically symmetric structures of oxide-confined VCSELs, using the model developed in Section 2 and the model parameters determined in Section 3.

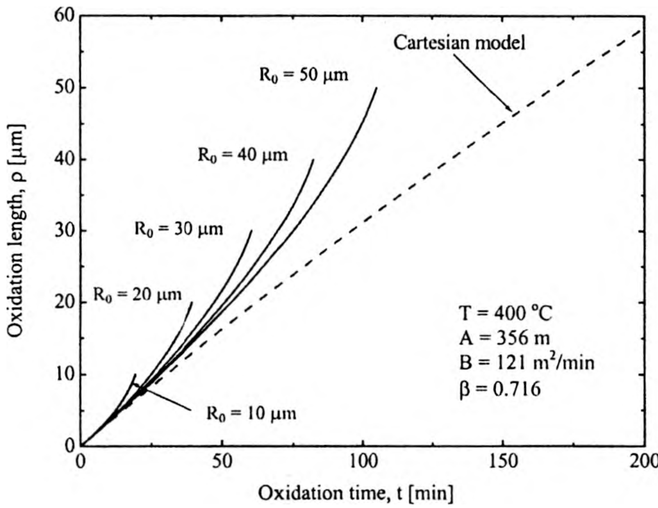

Fig. 3. Comparison of AlAs oxidation process kinetics ($d = 25$ nm) at 400 °C in cylindrical structures of various radii R_0 (solid lines) and the 1D Cartesian model (broken lines).

Until now, practically only the simplified 1D Cartesian model of the AlAs oxidation kinetics has been available. Therefore, it is interesting first to compare it with our model intentionally developed for the cylindrical mesa structure of VCSELs. Such a comparison is seen in Fig. 3, presenting (for various mesa radii R_0) plots of the oxidation length ρ versus the oxidation time t, calculated for a relatively thin ($d = 25$ nm) AlAs layer oxidized at 400 °C. Each curve is finished

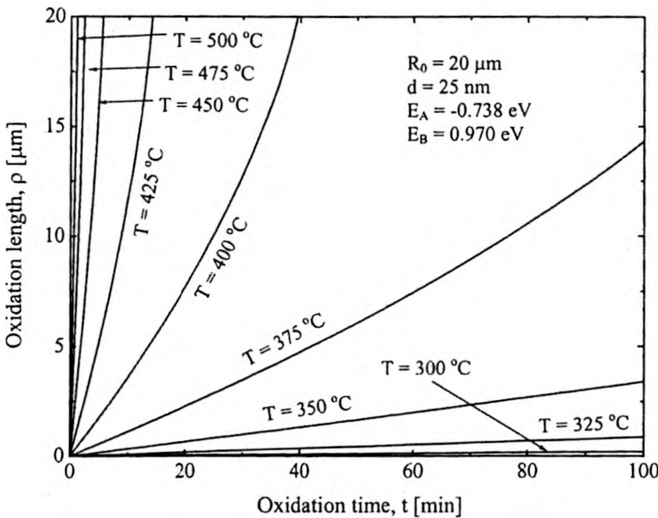

Fig. 4. Oxidation length ρ in a cylindrical mesa of radius $R_0 = 20$ μm with the AlAs layer thickness $d = 25$ nm versus oxidation time t for steam oxidation of AlAs conducted at various temperatures.

for $\rho = R_0$. As one can see, the 1D Cartesian model consistently underestimates the time required to reach a desired length of the oxidized region in a cylindrical structure and a significant difference is observed between predictions of both the models.

Figure 4 shows temperature sensitivity of the oxidation process of the 40-μm mesa ($R_0 = 20$ μm) in a thin (25 nm) AlAs layer. As expected, the initial slope of the $\rho(t)$ curves increases rapidly with temperature, which is directly associated with the activation energy $E_{B/A} = 1.7084$ eV (*cf.* Eq. (20)). Between 400 °C and 525 °C, the initial reaction rate increases by a factor of 100. Therefore, higher oxidation temperatures result in a substantial reduction of the oxidation time necessary to produce an assumed oxide aperture, while simultaneously rendering the control of the oxidation process much more dificult. It is also important to notice that at a temperature being too low ($T \leqslant 300$ °C) the AlAs oxidation process is extremely slow.

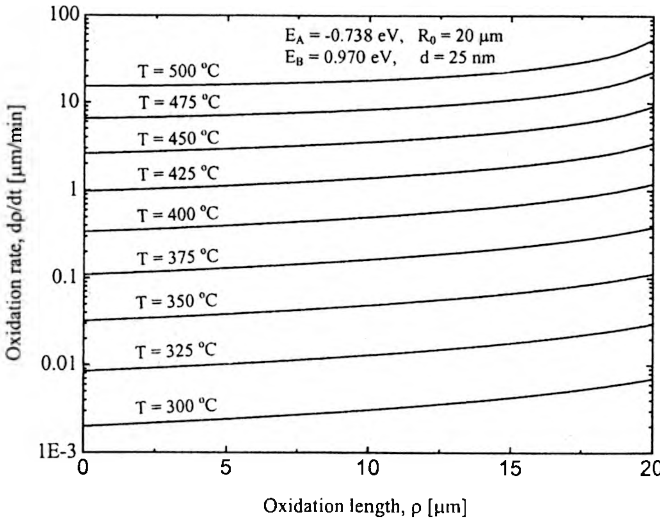

Fig. 5. Plots of the oxidation rate $d\rho/dt$ versus the oxidation length ρ (in a logarithmic scale) for an oxidation at various temperatures of the thin layers ($d = 25$ nm) of AlAs in a cylindrical mesa of radius $R_0 = 20$ μm.

An increase in the initial oxidation rate with temperature is also clrearly seen in Fig. 5 presenting (in a logarithmic scale) plots of the oxidation rate of the 25-nm AlAs layer in the 40-μm mesas versus the oxidation length. During the whole oxidation process, it was accelerated with an increase in ρ, which is consistent with plots shown in Fig. 2**b**.

Figure 6 reveals a very interesting dependence of the oxidation process on the AlAs layer thickness d. In the range of thicknesses shown in Fig. 6, the initial oxidation rate B/A increases monotonically with increasing d. However, for d larger than 100 nm (*cf.* also Fig. 2**a** and Fig. 2**b**), the oxidation process becomes slower as

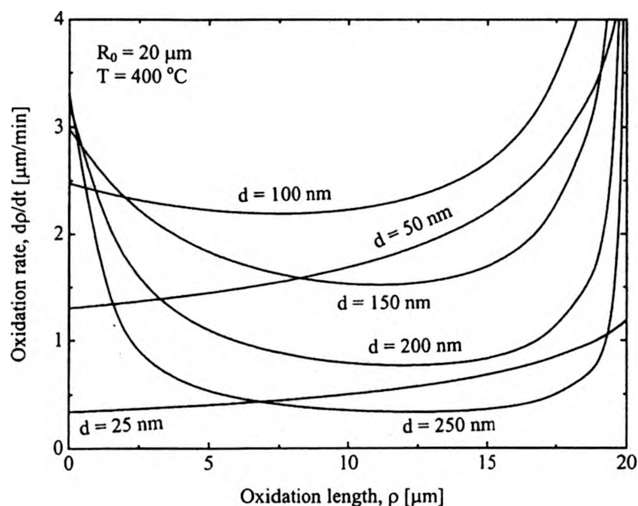

Fig. 6. Oxidation rate $d\rho/dt$ versus the oxidation length ρ for cylindrical mesas of R_0 = 20 µm and various AlAs layer thicknesses, steam oxidized at 400 °C.

the oxidation front moves further into the AlAs layer. The complete oxidation time t_c may be obtained by setting $\rho = R_0$ to Eq. (7)

$$t_c = \frac{R_0}{2B}[(2-\beta)A + R_0]. \tag{22}$$

It is possible to find the AlAs layer thickness d_c, at which t_c reaches the minimum. The resultant equation is transcendental, and for parameters determined in Section 3 for 400 °C we obtain $d_c = 93.4$ nm, consistent with the picture presented in Fig. 6.

The initial oxidation rate B/A also has a nonmonotonic character, reaching a maximum at a thickness d_{max} larger than those shown in Fig. 6. Equations (17)–(19) give the following analytical result for d_{max}:

$$d_{max} = \sqrt{\frac{(\varepsilon_{EB} - \varepsilon_{EA}) d_{A0} d_{B0}}{k_B T (d_{A0} - d_{B0})}}. \tag{23}$$

Using values of the parameters given in Section 3, we obtain $d_{max} =$ 290.1 nm at 400 °C.

5. Conclusions

In this paper, compact analytical formulae describing the kinetics of the AlAs steam oxidation process in cylindrically symmetric mesa structures have been derived and discussed. The process parameters have been determined by fitting our theoretical curves into experimental results. The parameters have been found to be strongly dependent on both the AlAs layer thickness and temperature.

We show that significant differences exist between the prediction of the cylindrical model and those of the one-dimensional Cartesian model that has been widely used up to date. Our detailed model can therefore be very important for achieving a good control of the oxidation process in cylindrically symmetric VCSEL structures.

Acknowledgments – This work was supported by the US – Poland Maria Skłodowska-Curie Joint Fund grant No. MEN/NSF-98-336, by the Polish State Committee for Scientific Research (KBN), grants Nos. 7-T11B-069-20, 7-T11B-073-21, by DARPA under the Optoelectronic Materials Center program, and by the CFD Research Corporation.

References

[1] DALLESASSE J. M., GAVRILOVIC P., HOLONYAK N., Jr., KALISKI R. W., NAM D. W., VESELY E.J., BURNHAM R.D., Appl. Phys. Lett. **56** (1990), 2436.
[2] DALLESASSE J. M., HOLONYAK N., Jr., SUGG A. R., RICHARD T. A., EL-ZEIN L., Appl. Phys. Lett. **57** (1990), 2844.
[3] CHOQUETTE K. D., SCHNEIDER R. P., Jr., LEAR K. L., GEIB K. M., Electron. Lett. **30** (1994), 2043.
[4] CHOQUETTE K. D., GEIB K. M., ASHBY C. I.H., TWESTEN R. D., BLUM O., HOU H.Q., FOLLSTAEDT D. M., HAMMONS B., MATHES D., HULL R., IEEE Sel. Topics Quantum Electron. **3** (1997), 916.
[5] DEPPE D. G., HUFFAKER D. L., Proc. SPIE CR**70** (1998), 141.
[6] HUFFAKER D. L., DEPPE D. G., KUMAR K., ROGERS T. J., Appl. Phys. Lett. **65** (1994.) 97.
[7] JUNG C., JGER R., GRABHERR M., SCHNITZER P., MICHALZIK R., WEIGL B., MLLER S., EBELING K .J., Electron. Lett. **33** (1997), 1790.
[8] MACDOUGAL M. H., GESKE J., LIN C. K., BOND A.E., DAPKUS P. D., IEEE Photon. Technol. Lett. **10** (1998), 9.
[9] YANG G. M., LIM D. H., KIM J. H., LIM K. Y., LEE H J., Jpn. J. Appl. Phys. Pt. 1, **37** (1998,) 1391.
[10] KOLEY B., DAGENAIS M., JIN R., PHAM J., SIMONIS G., MCLANE G., STONE D., J. Appl. Phys. **82** (1997), 4586.
[11] ALONZO A. C., CHENG X.-C., MCGILL T. C., J. Appl. Phys. **84** (1998), 6901.
[12] DEAL B. E., GROVE A. S., J. Appl. Phys. **36** (1965), 3770.
[13] OCHIAI M., GIUDICE G. E., TEMKIN H., SCOTT J. W., COCKERILL T. M., Appl. Phys. Lett. **68** (1996), 1898.
[14] NAONE R. L., COLDREN L. A., J. Appl. Phys. **82** (1997), 2277.
[15] KIM J.-H., LIM D. H., KIM K .S., YANG G. M., LIM K. Y., LEE H. J., Appl. Phys. Lett. **69** (1996), 3357.
[16] LAGENFELDER T., SCHRDER S., GROTHE H., J. Appl. Phys. **82** (1997), 3548.
[17] YOSHIKAWA T., SAITO H., KOSAKA H., SUGIMOTO Y., KASAHARA K., Appl. Phys. Lett. **72** (1998), 2310.

Received October 9, 2000